Regional Seismic Characteristics of Chemical Explosions on the Eastern Margin of the Junggar Basin, Northwest China, and of Historical Semipalatinsk Nuclear Tests

Xiao Ma[1,2], Lian-Feng Zhao[*1], Xiao-Bi Xie[3], Xi He[1], and Zhen-Xing Yao[1]

ABSTRACT

The applicability of the empirical magnitude–yield relations developed for northeast China and Korean Peninsula explosions was investigated for data from northwest China. We collected regional broadband digital seismic data from 13 chemical explosions (CEx) detonated between 6 September and 10 October 2018, on the eastern margin of the Junggar basin, northwest China, five nuclear tests at the Semipalatinsk nuclear test site, and eight natural earthquakes. Both *Lg* and Rayleigh-wave magnitudes ($m_b(Lg)$ and M_s, respectively) were estimated for these events. Similar to the North Korean test site, the $m_b(Lg)$–M_s discriminant did not properly distinguish explosions from natural earthquakes at the Semipalatinsk test site. However, network-averaged *P*/*S* spectral ratios (*Pg*/*Lg*, *Pn*/*Lg*, and *Pn*/*Sn*) did successfully discriminate explosions from earthquakes at both the North Korean and the Semipalatinsk test sites at frequencies above 2.0 Hz. Based on 13 known-yield CEx, we selected an empirical magnitude–yield relation to constrain the explosive yields of five historical nuclear tests at the Semipalatinsk test site. The resulting yields are lower than those previously obtained from teleseismic observations.

KEY POINTS

- Regional nuclear monitoring techniques are evaluated with a new chemical explosion dataset in northwest China.
- The network measured *P*/*S* spectral ratio is a good discriminant but the $m_b(Lg)$–M_s is not in northwest China.
- Several ground-truth events are provided for reevaluating the historic Semipalatinsk nuclear tests.

INTRODUCTION

Seismology plays the most important role in the family of explosion monitoring technologies consisting mainly of seismological, infrasound, hydroacoustic, and radionuclide methods employed to detect, locate, and characterize underground nuclear tests (Argo *et al.*, 1995; Barazangi *et al.*, 1996; Steinberg and Rabinowitz, 2003; Xie and Zhao, 2018; Gaebler *et al.*, 2019). With the reduction in test yields over the past several decades, the signal-to-noise ratio of teleseismic data is often too low to obtain high quality seismic records. Therefore, monitoring methods have shifted from using global network data (Marshall and Basham, 1973; Ringdal *et al.*, 1992) to seismic data acquired at regional distances (Koper, 2020).

Since 2006, North Korea has conducted six underground nuclear tests at the North Korean test site (NKTS) of Punggye-ri, leading to the rapid development of regional monitoring techniques involving new magnitude measurements (Bonner *et al.*, 2008, 2011; Hong *et al.*, 2008; Shin *et al.*, 2010; Chun *et al.*, 2011; Fan *et al.*, 2013; Zhang and Wen, 2013; Zhao, Xie, He, *et al.*, 2017; Zhao, Xie, Wang, *et al.*, 2017), yield estimation (Zhao *et al.*, 2008, 2012, 2014; Rougier *et al.*, 2011; Murphy *et al.*, 2013; Zhang and Wen, 2013; Zhao *et al.*, 2016; Zhao, Xie, He, *et al.*, 2017; Pasyanos and Myers, 2018; Voytan *et al.*, 2019), and event discrimination (Kim and Richards, 2007; Zhao *et al.*, 2008, 2014, 2016; Zhao, Xie, He, *et al.*, 2017; Zhao, Xie, Wang, *et al.*, 2017; Walter *et al.*, 2018). However, because of the limited coverage of explosion data and the particular lack of available published

1. Key Laboratory of Earth and Planetary Physics, Institute of Geology and Geophysics, Chinese Academy of Sciences, Beijing, China; 2. University of Chinese Academy of Sciences, Beijing, China; 3. Institute of Geophysics and Planetary Physics, University of California at Santa Cruz, Santa Cruz, California, U.S.A.

*Corresponding author: zhaolf@mail.iggcas.ac.cn

Cite this article as Ma, X., L.-F. Zhao, X.-B. Xie, X. He, and Z.-X. Yao (2020). Regional Seismic Characteristics of Chemical Explosions on the Eastern Margin of the Junggar Basin, Northwest China, and of Historical Semipalatinsk Nuclear Tests, *Bull. Seismol. Soc. Am.* **111**, 606–620, doi: 10.1785/0120200151

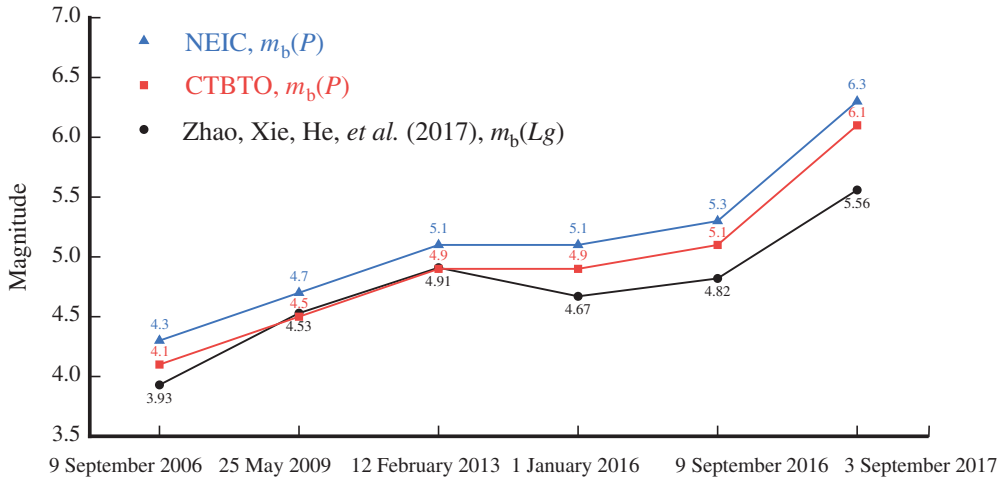

Figure 1. Comparison of the body-wave magnitudes for the North Korean test site (NKTS) nuclear tests from different sources. The $m_b(P)$ values are from the U.S. Geological Survey (USGS) National Earthquake Information Center (NEIC) and the Comprehensive Test Ban Treaty Organization (CTBTO), and the $m_b(Lg)$ values are obtained from Zhao, Xie, He, *et al.* (2017).

yields for regional events, some monitoring results are inconsistent. For example, the values of the regional body-wave magnitude $m_b(Lg)$ and teleseismic body-wave magnitude $m_b(P)$ illustrated in Figure 1 are calculated for six nuclear tests at the NKTS. The $m_b(Lg)$ obtained by Zhao, Xie, He, *et al.* (2017) is approximately 0.2 magnitude units (m.u.) lower than the $m_b(P)$ from the Comprehensive Test Ban Treaty Organization and 0.4 m.u. lower than that from the U.S. Geological Survey National Earthquake Information Center. One possibility for this is that the empirical replacement of $m_b(P)$ with $m_b(Lg)$ based on earthquake data may underestimate the magnitude of an explosion. Data from new explosions and historical nuclear tests, such as those in northwest China and its surrounding areas, may provide clues regarding this possibility and further improve seismic monitoring techniques based on regional observations. Based on the assumption that $m_b(Lg)$ and $m_b(P)$ are interchangeable, Zhao *et al.* (2016) adopted the fully coupled hard-rock site empirical equation given by Bowers *et al.* (2001) for Novaya Zemlya to estimate the explosion yields in the Korean Peninsula. It is therefore worth testing whether the empirical equation from northeast China and the Korean Peninsula is applicable to northwest China and its neighboring areas. In addition, many investigations have pointed out that the m_b–M_s method cannot efficiently discriminate between events in northeast China and the Korean Peninsula (Bonner *et al.*, 2008; Chun *et al.*, 2011; Murphy *et al.*, 2013; Zhao, Xie, Wang, *et al.*, 2017), whereas the regional *P*/*S* (*Pn*/*Lg*, *Pn*/*Sn*, *Pg*/*Lg*, and *Pg*/*Sn*) spectral ratio method (Kim and Richards, 2007; Zhao *et al.*, 2008, 2014; Zhao *et al.*, 2016; Zhao, Xie, He, *et al.*, 2017; Zhao, Xie, Wang, *et al.*, 2017; Walter *et al.*, 2018) can effectively separate explosions from earthquakes. However, the applicability of these empirical formulas to northwest China and its neighboring areas still needs to be verified based on regional seismic observations from this region.

In this study, we used seismic data from 13 chemical explosions (CEx) originally implemented for reflection seismic surveying and deep seismic sounding profiling on the eastern margin of the Junggar basin, Xinjiang, northwest China, to investigate the discrimination of explosion events and the estimation of yields. We also examined seismic data from five historical nuclear tests at the Semipalatinsk nuclear test site (SNTS) in the Soviet Union and eight natural earthquakes (NEqs), of which six were close to the Junggar CEx and two were near the SNTS (Fig. 2). By calculating $m_b(Lg)$ and the surface (Rayleigh)-wave magnitude M_s, we estimated the explosive yields for the Semipalatinsk nuclear tests (SNTs) and examined the applicability of m_b–M_s in discriminating events in northwest China and its neighboring regions. We also revisited the network-averaged *P*/*S* spectral ratio method, which was originally developed in northeast China for North Korean tests, and investigated its potential applicability in northwest China.

REGIONAL DATASETS

Between 6 September and 10 October 2018, 13 three-ton CEx were detonated by the Geophysical Exploration Center, China Earthquake Administration, for reflection seismic surveying and deep sounding purposes along a 600 km profile on the eastern margin of the Junggar basin, northwest China. The event parameters are listed in Table 1. These explosions were recorded by 122 broadband digital stations from several regional networks, including the China National Digital Seismic Network, Global Seismic Network, and International Federation of Digital Seismic Networks. We selected 851 vertical seismograms from these 13 CEx, five underground nuclear tests at the SNTS, and eight nearby earthquakes to investigate the characteristics of explosion sources in this area, including the magnitude–yield relation, and to discriminate between explosions and earthquakes.

As an example, Figure 3 shows the broadband vertical-component velocity seismograms for the 13 CEx recorded at station BTS. Their waveforms are highly consistent and characterized by abrupt *P*-wave arrivals and relatively weak *Lg* phases. In

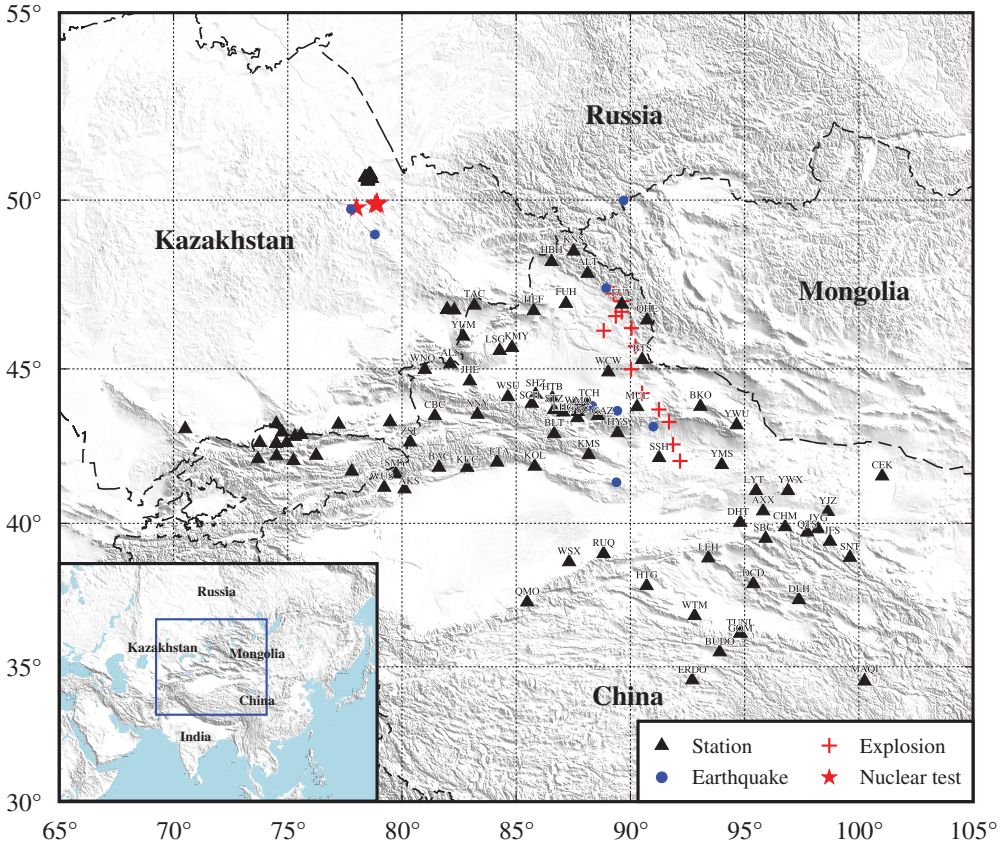

Figure 2. Topographic map showing the study area in northwest China and its neighboring regions. Superimposed on the map are the locations of nuclear explosions (solid red stars) at the SNTS, 13 chemical explosions (red crosses), six nearby earthquakes (solid blue circles), and seismic stations (solid black triangles) from the China National Digital Seismic Network (CNDSN), Global Seismic Network (GSN), and International Federation of Digital Seismograph Networks (FDSN). The blue square in the inset map delineates the location of the study area.

contrast, Figure 4 shows similar records for six earthquakes that occurred nearby with waveforms that are typically enriched in *S*-wave energy. Furthermore, Figure 5 displays the velocity seismograms generated by a CEx detonated at 19:20 on 25 September 2018, which was recorded by stations at distances between 100 and 530 km. Strong *P*-wave energy and relatively weak *Lg* phases can be seen on these waveforms, especially for the remote stations. Figure 6 illustrates the velocity seismograms recorded at station WMQ, generated by the five SNTs and two nearby tectonic earthquakes. For the explosion waveforms, only *P* waves can be observed clearly because explosions release a large amount of compressional energy, whereas the energies of other regional phases, for example, *Sn*, *Lg*, and short-period Rayleigh waves, are too weak to be identified in normalized seismograms. On the other hand, the earthquake seismograms show relatively weak *P* waves and strong *Lg* waves due to their dislocation source mechanism. Different excitations of *P*- and *S*-type waves from these two types of sources form the basis for the event discrimination method presented herein.

EVENT MAGNITUDE AND YIELD ESTIMATION

Both $m_b(Lg)$ and M_s were calculated from *Lg* and Rayleigh waves. Following Zhao *et al.* (2008, 2012), the third peak (TP) amplitude method (Nuttli, 1973, 1986) and root mean square (rms) amplitude method (Patton and Schlittenhardt, 2005) were both used to calculate $m_b(Lg)$ with

$$m_b(Lg) = 5.0 + \log_{10}[A(\Delta_0)/C], \quad (1)$$

in which $A(\Delta_0)$ and C are the *Lg*-wave amplitudes at a reference distance $\Delta_0 = 10$ km for an unknown magnitude event and an m_b 5.0 event, respectively. The values of the constant C are 110 and 90 μm for the TP and rms methods, respectively (Nuttli, 1973, 1986; Patton and Schlittenhardt, 2005). To calculate the amplitude $A(\Delta_0)$, we extrapolate the observed *Lg*-wave amplitude $A(\Delta)$ at an epicentral distance Δ from the unknown magnitude event using

$$A(\Delta_0) = A(\Delta)G(\Delta, \Delta_0)\Gamma(\Delta, \Delta_0, f), \quad (2)$$

in which $G(\Delta, \Delta_0)$ is the geometrical spreading from Δ to Δ_0. For the TP method (Nuttli, 1973, 1986),

$$G(\Delta, \Delta_0, \mathrm{TP}) = (\Delta/\Delta_0)^{1/3}[\sin(\Delta/111.1)/\sin(\Delta_0/111.1)]^{1/2}, \quad (3)$$

and for the rms method (Yang, 2002; Patton and Schlittenhardt, 2005),

$$G(\Delta, \Delta_0, \mathrm{rms}) = (\Delta/\Delta_0)^{1.0}. \quad (4)$$

In equation (2),

$$\Gamma(\Delta, \Delta_0, f) = \exp\left[-\frac{\pi f}{V}\int_{\Delta_0}^{\Delta}\frac{ds}{Q(x, y, f)}\right], \quad (5)$$

is the attenuation factor, in which f is the frequency, V is the *Lg*-wave group velocity, $\int_{\Delta_0}^{\Delta} ds$ is the integral along the great

TABLE 1
Event Parameters Used in This Study

Explosions and Earthquakes		Date and Origin Time (yyyy/mm/dd hh:mm:ss.ss)	Latitude (° N)	Longitude (° E)	Depth (km)	$m_b(P)$ or Yield (ton)	Source Rock Environment	Magnitude Measurements					
								$m_b(Lg)$	St. Dev.	*N*	M_s	St. Dev.	*N*
Chemical explosion (CEx)	CEx01	2018/09/06 19:00:14.00	43.271	91.727	0.06	3 (ton)	Hard rock	2.15	0.22	13	—	—	—
	CEx02	2018/09/06 19:10:14.40	42.612	91.870	0.06	3 (ton)	Hard rock	2.05	0.25	15	—	—	—
	CEx03	2018/09/06 19:20:13.20	42.069	92.178	0.06	3 (ton)	Hard rock	1.82	0.29	8	—	—	—
	CEx04	2018/09/14 19:20:13.30	43.679	91.333	0.06	3 (ton)	Hard rock	1.85	0.38	9	1.56	0.27	9
	CEx05	2018/09/15 19:00:43.00	44.986	90.029	0.06	3 (ton)	Hard rock	2.37	0.16	40	1.97	0.51	25
	CEx06	2018/09/15 19:10:14.20	44.241	90.512	0.06	3 (ton)	Loess	2.52	0.19	44	1.88	0.29	37
	CEx07	2018/09/18 19:10:14.10	46.250	90.049	0.06	3 (ton)	Hard rock	2.02	0.12	14	1.83	1.10	13
	CEx08	2018/09/18 19:20:13.20	45.701	90.226	0.06	3 (ton)	Hard rock	1.91	0.18	10	1.55	0.	1
	CEx09	2018/09/25 19:00:14.60	46.745	89.620	0.06	3 (ton)	Hard rock	2.03	0.19	12	1.51	0.26	16
	CEx10	2018/09/25 19:20:13.30	47.386	89.364	0.06	3 (ton)	Hard rock	2.05	0.13	18	1.79	0.71	17
	CEx11	2018/10/09 12:25:42.00	47.066	89.962	0.06	3 (ton)	Hard rock	2.10	0.11	15	1.51	0.22	14
	CEx12	2018/10/10 06:43:39.00	46.616	89.363	0.06	3 (ton)	Hard rock	1.93	0.15	7	1.32	0.37	9
	CEx13	2018/10/10 09:53:10.00	46.172	88.317	0.06	3 (ton)	Gravel	1.90	0.70	7	1.34	0.49	6
Natural earthquake (NEq)	NEq1	2012/01/01 08:07:01.75	49.742	77.766	10.00	m_b 4.2	—	3.82	0.89	144	2.77	0.28	69
	NEq2	2015/01/20 09:30:55.25	49.019	78.818	10.00	m_b 4.9	—	5.16	0.82	134	3.41	0.50	65
	NEq3	2013/07/19 10:58:08.61	47.454	88.939	10.00	m_b 4.7	—	5.23	0.54	116	3.05	0.42	58
	NEq4	2014/10/20 03:57:26.91	43.837	88.329	30.38	m_b 4.6	—	5.11	0.32	178	2.85	0.50	88
	NEq5	2016/03/29 14:57:12.10	41.371	89.386	21.06	m_b 4.8	—	5.19	0.37	110	3.03	0.66	55
	NEq6	2016/07/13 06:45:47.88	49.991	89.699	10.00	m_b 4.8	—	5.37	0.51	96	3.61	0.62	46
	NEq7	2016/08/15 23:59:51.51	43.685	89.429	22.01	m_b 4.1	—	4.10	0.39	134	2.26	0.80	65
	NEq8	2016/08/20 10:27:30.70	43.176	91.005	10.00	m_b 4.1	—	4.80	0.37	48	3.37	0.	2
Semipalatinsk nuclear test (SNT)	SNT1	1988/04/03 01:33:09.70	49.908	78.908	—	m_b 6.1†	—	5.77	0.00	2	3.79	0.00	1
	SNT2	1988/09/14 04:00:03.40	49.878	78.823	0.65*	m_b 6.1†	—	5.67	0.02	2	3.84	0.00	1
	SNT3	1988/10/18 03:40:07.50	49.780	78.008	0.13*	m_b 4.9†	—	4.29	0.01	2	2.32	0.00	1
	SNT4	1988/12/17 04:18:09.60	49.882	78.925	0.64*	m_b 5.9†	—	5.50	0.01	2	3.72	0.00	1
	SNT5	1989/10/19 09:50:00.60	49.922	78.908	—	m_b 6.0†	—	5.46	0.03	2	3.77	0.00	1

N, the number of recordings for calculating the average; St. dev., standard deviation.
*From Stevens *et al.* (2007).
†From the United Kingdom Atomic Weapons Establishment (AWE).

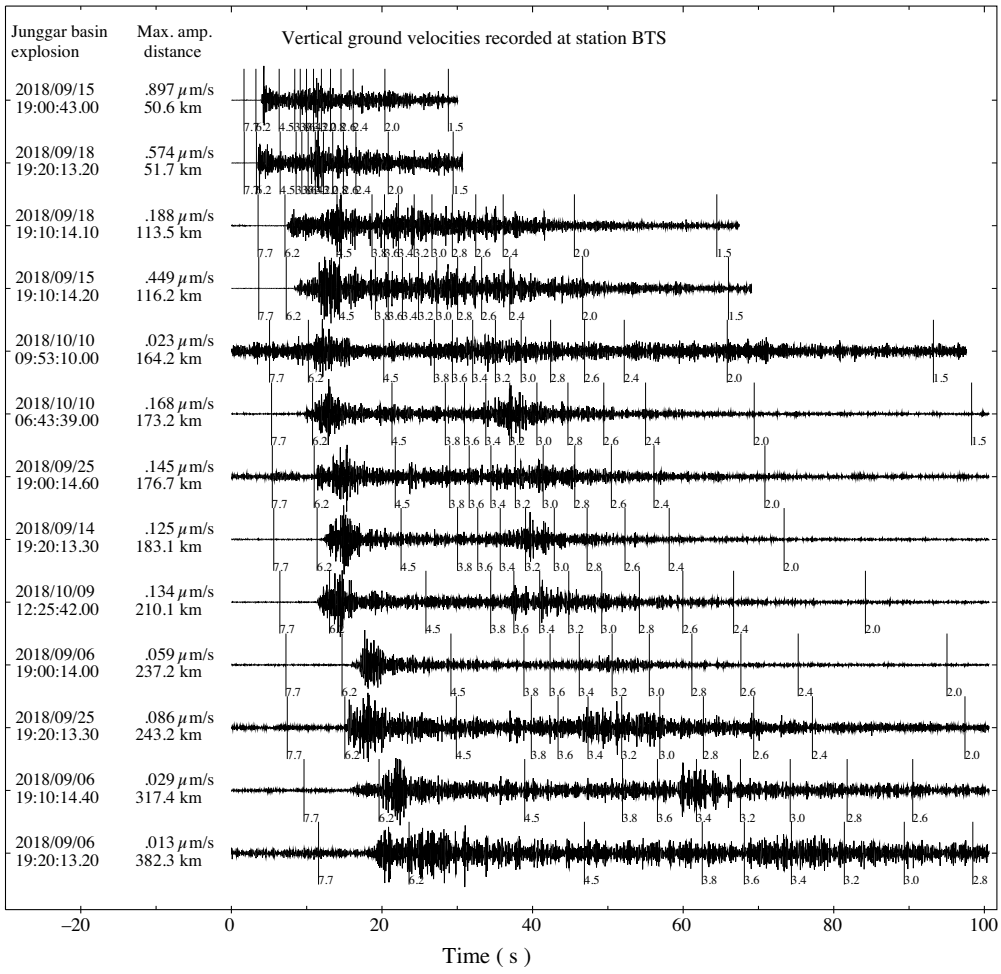

Figure 3. Normalized vertical-component velocity seismograms band-passed between 5.0 and 10.0 Hz for the 13 chemical explosions detonated on the eastern margin of the Junggar basin and recorded at station BTS in northwest China. The group velocities are labeled for different regional phases.

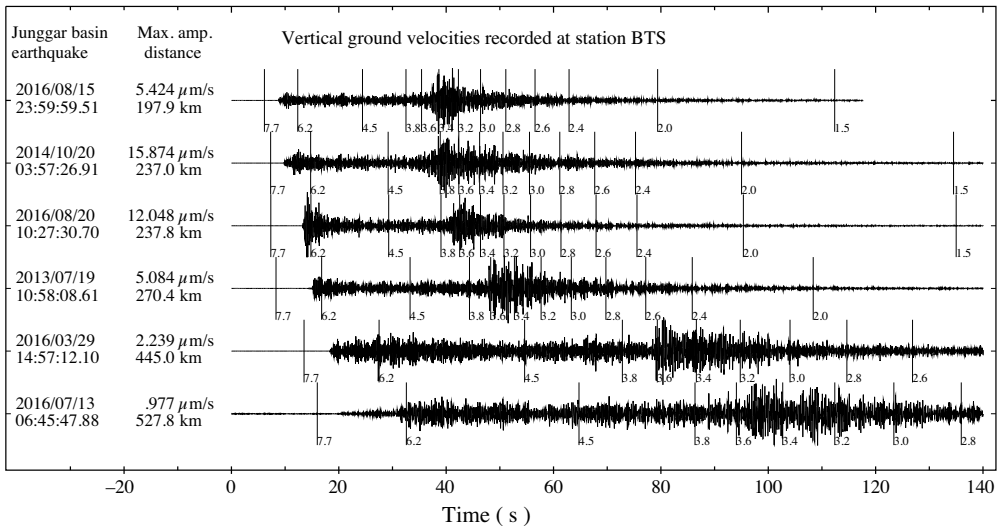

Figure 4. This is the same as Figure 3 except for six natural earthquakes near chemical explosions.

circle wavepath from Δ_0 to Δ, and $Q(x, y, f)$ is the quality factor of crustal media, a function of the frequency and surface location (x, y). For the attenuation correction in calculating the *Lg*-wave magnitude, we developed a high-resolution broadband *Lg*-wave attenuation model (Fig. 7) for northwest China using a large regional dataset (Zhao *et al.*, 2018).

The procedure to calculate the *Lg*-wave magnitude is as follows:

1. Deconvolve the instrument response from the observed broadband vertical-component velocity seismograms.
2. Simulate the short-period records by convolving the WWSSN-short-period instrument response with the ground-motion seismograms.
3. Pick the *Lg*-wave arrivals using a group velocity window between 3.6 and 3.0 km/s.
4. Measure both the TP amplitude and the rms amplitude and correct the rms amplitude for pre-P noise (Zhao *et al.*, 2008).
5. Extrapolate the observed amplitude to the reference distance using equations (2)–(4) and the *Lg*-wave attenuation model (Zhao *et al.*, 2018).
6. Use 3.5 km/s as the *Lg*-wave group velocity and calculate the dominant frequency by counting the zero crossings.
7. Calculate the *Lg*-wave magnitude with both the TP and the rms methods based on equation (1).

After correcting the magnitudes with station terms, we

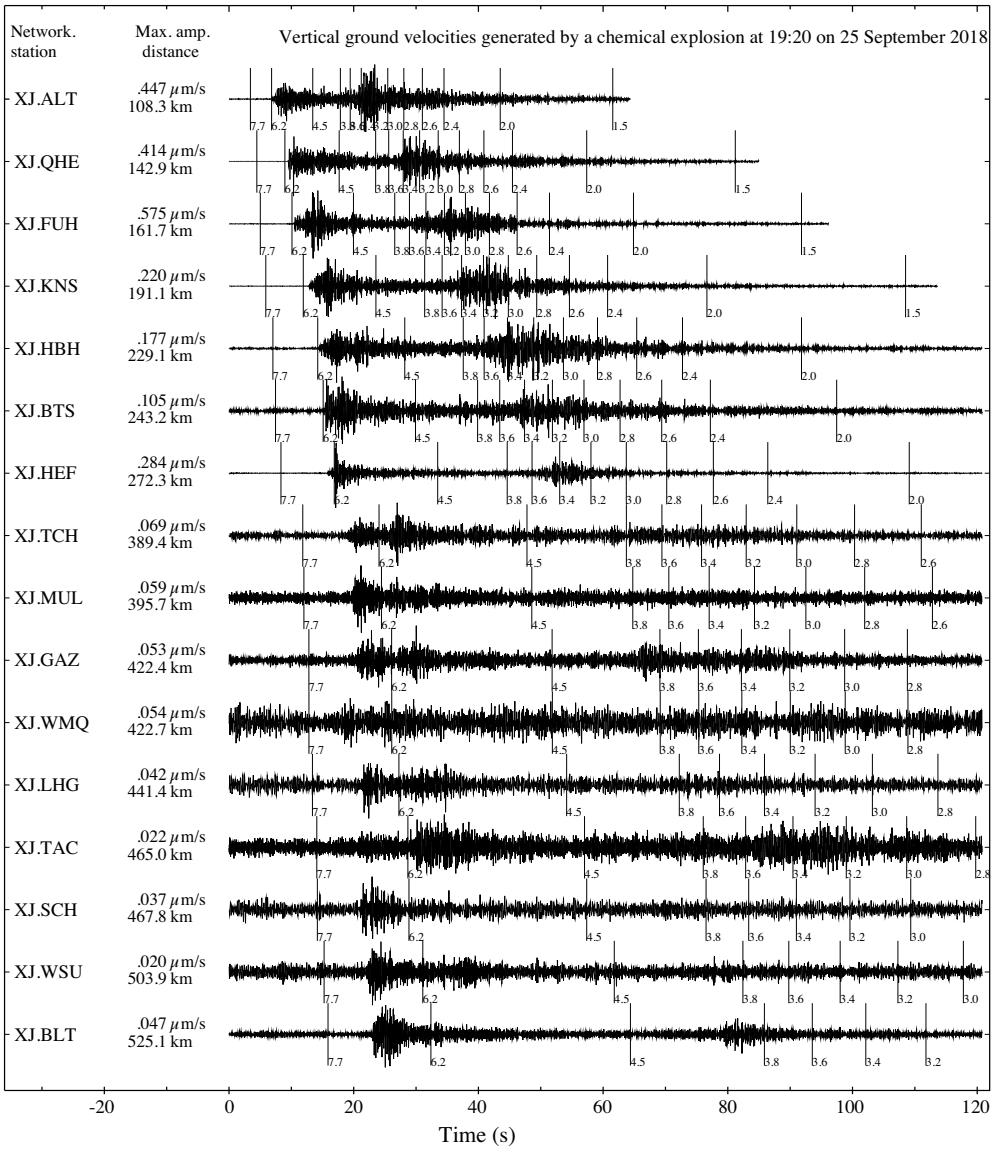

Figure 5. This is the same as Figure 3 except for a chemical explosion that occurred at 19:20 on 25 September 2018, recorded by stations in the Xinjiang network.

took the network-averaged values of both the $m_b(Lg, \mathrm{TP})$ and the $m_b(\mathrm{Lg}, \mathrm{rms})$ measurements as the resulting body-wave magnitudes for all events. Table 2 lists the observed TP and rms amplitudes of *Lg* waves at station WMQ from the five SNTs as well as the frequency, path *Q* values, calibrated *Lg* amplitudes at 10 km, calculated magnitudes based on equation (1), and magnitudes of *Lg* waves corrected by site responses. Taking the averages of both the $m_b(Lg, \mathrm{TP})$ and the $m_b(Lg, \mathrm{rms})$ measurements, we determined the *Lg*-wave magnitudes for SNT1–5 to be $m_b(Lg) = 5.77$, 5.67, 4.29, 5.49, and 5.46 (Table 1).

In addition, we calculated M_s using a time-domain method (Russell, 2006) that not only extends the applicability of M_s to regional distances but also extends the usable frequency range for magnitude-defining observations. This method has been validated in different regions for low-magnitude events (Bonner *et al.*, 2006), and consistent results were obtained by different authors for North Korean nuclear tests at both teleseismic and regional distances (Bonner *et al.*, 2008; Chun *et al.*, 2011; Fan *et al.*, 2013; Murphy *et al.*, 2013). The Rayleigh-wave magnitudes obtained for SNT1–5 are $M_s = 3.79$, 3.84, 2.32, 3.72, and 3.77 (Table 1).

For $m_b(Lg)$, Table 3 compares our results with those previously obtained by Ringdal *et al.* (1992), in which a systematic bias of ~0.3 m.u. is shown. For these nuclear tests, we used only one station WMQ in this study, which may lead to biased magnitude measurements. On the other hand, we used a recently developed broadband *Lg*-wave *Q* model to correct for the attenuation effect that can improve the $m_b(Lg)$ estimates. Nevertheless, it is still a challenge to convert the *P*-wave magnitude into the *S*-wave magnitude. Based on the $m_b(Lg)$ measurements, we adopted empirical magnitude–yield relations to estimate the seismic yields of the SNTs (Nuttli, 1986; Ringdal *et al.*, 1992; Murphy, 1996; Bowers *et al.*, 2001). Figure 8 shows the $m_b(Lg)$–yield relations for the Nevada test site (Nuttli, 1986), Novaya Zemlya (Bowers *et al.*, 2001), and East Kazakhstan (Ringdal *et al.*, 1992; Murphy, 1996). The 13 small CEx, each detonated using three tons of explosive ammonium nitrate, are also plotted in Figure 8. These explosions may provide reliable references at the low-yield end when choosing an empirical magnitude–yield relation for the SNTS. For these CEx, the reported yield is the weight of the ammonium nitrate explosive. Because this kind of explosive is less powerful than trinitrotoluene (TNT), we assume that its relative effective factor is roughly half that of TNT (Zhao *et al.*, 2014). On the other hand, according to the result from the non-proliferation experiment, CEx are more efficient at generating seismic signals than nuclear tests by approximately a factor of 2 (Denny *et al.*, 1996; Zhao

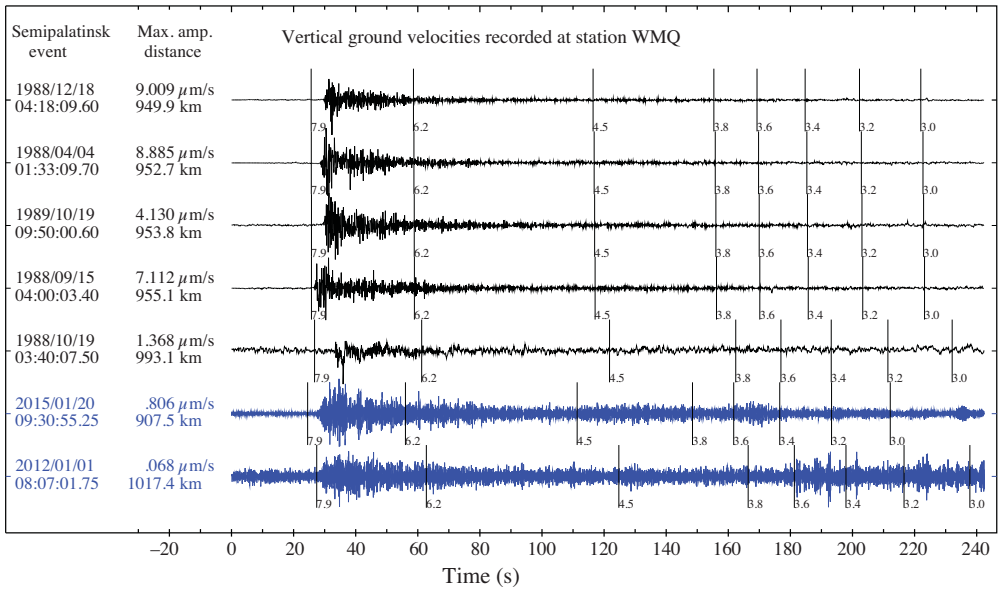

Figure 6. Normalized vertical-component velocity seismograms band-passed between 5.0 and 10.0 Hz recorded at station WMQ. Waveforms for five nuclear tests at the Semipalatinsk nuclear test site (SNTS) are shown in black and waveforms for two nearby earthquakes are shown in blue. The event dates, maximum amplitudes, and epicenter distances are listed on the left. Vertical lines on the waveforms indicate the apparent group velocities. The seismograms from the nuclear tests show clear impulsive *P*-wave onsets, but *Sn* and *Lg* phases are nearly invisible, whereas the seismograms for the nearby earthquakes are characterized by relatively weak *P* waves and relatively strong *Lg* waves due to their shear dislocation source mechanisms.

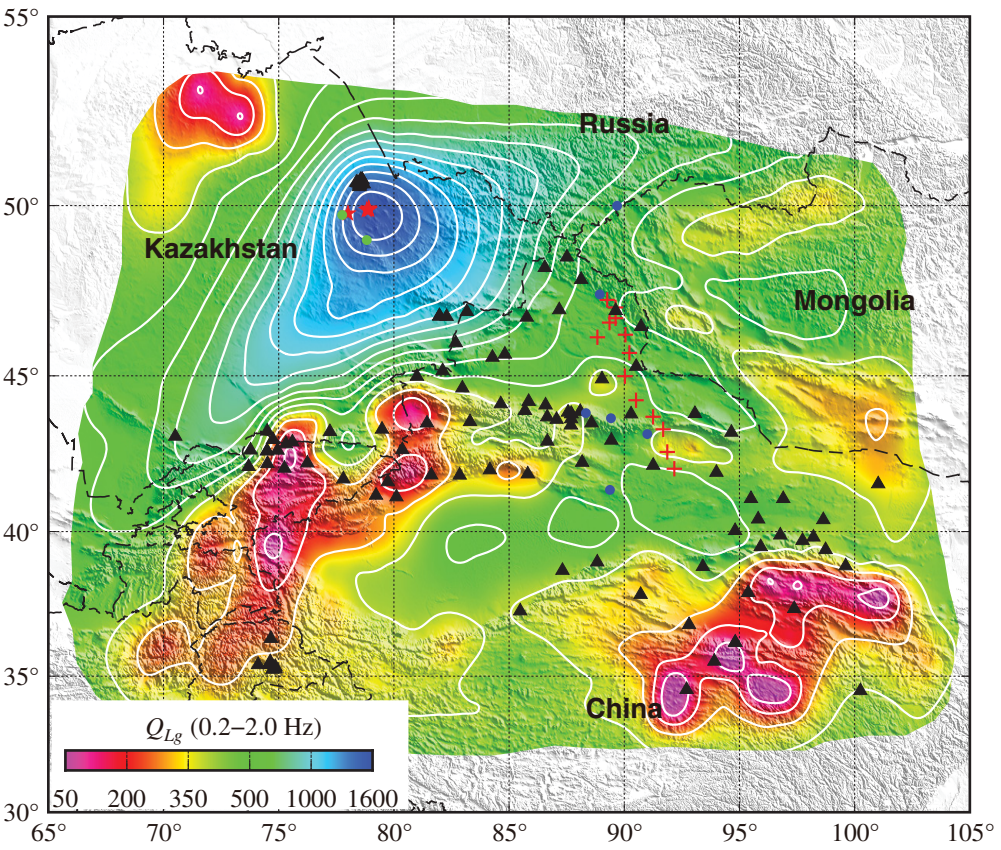

Figure 7. Broadband Q_{Lg} map between 0.2 and 2.0 Hz for the investigated region (Zhao *et al.*, 2018).

et al., 2014). Combining the previous two factors, for explosions that use ammonium nitrate as the main blasting agent, one ton of charge weight will generate seismic amplitudes approximately comparable to a nuclear test equivalent to a ton of TNT. Considering that the SNTS is located on a geologically stable platform and the constraint of known-yield small CEx at the low-yield end, we selected the fully coupled hard-rock site equation by Bowers *et al.* (2001) to estimate the yields of the SNTs (Zhao *et al.*, 2008). Using this equation, the yields estimated for SNT1–5 are 106.3, 78.2, 1.1, 45.0, and 4l.1 kt (Fig. 8). These values are based on the assumption that the nuclear tests were detonated at a scaled depth of $h_{\text{scaled}} = h_0 \cdot W^{1/3}$, in which $h_0 = 120$ m/kt$^{1/3}$ and W is the explosive yield. However, if the source was greatly overburied, these yields may be underestimated. Table 3 compares the yield estimations for the SNTs from different authors. The yields obtained here are smaller than those from both Ringdal *et al.* (1992) and Stevens *et al.* (2007). It is commonly accepted that the yield estimation can be affected by several factors, for example, uncertain burial depths, the replacement of global $m_b(P)$ with $m_b(Lg)$, and the local geology. According to the depth correction term, $-0.7875 \cdot \log_{10}(h/h_{\text{scaled}})$, suggested by Patton and Taylor (2011), we adjusted the yields for three of the five SNTs using the burial depths estimated by Stevens *et al.* (2007), as shown in Table 3. The estimated yields from the present research are approximately 63% of those

TABLE 2
Magnitude and Yield Estimations Using the Third Peak Method and Rms Amplitudes of *Lg* Waves at Station WMQ

Semipalatinsk Nuclear Test (SNT)	Date and Origin Time (yyyy/mm/dd hh:mm:ss.ss)	Distance (km)	Measured A (Δ)(μm)		Measured $f(Lg)$	Path Q	A(10 km) (μm)		$m_b(Lg)$		Corrected $m_b(Lg)$		Yield (kt)	
			TP	rms			TP	rms	TP	rms	TP	rms	TP	rms
SNT1	1988/04/03 01:33:09.70	952.7	2.523	0.977	0.833	849	257.560	213.477	5.37	5.38	5.74	5.80	96.98	116.59
SNT2	1988/09/14 04:00:03.40	955.1	1.922	0.790	0.829	856	194.899	171.658	5.25	5.28	5.62	5.71	67.09	88.44
SNT3	1988/10/18 03:40:07.50	993.1	0.073	0.029	1.162	1115	8.408	7.165	3.88	3.90	4.26	4.33	1.03	1.28
SNT4	1988/12/17 04:18:09.60	949.9	1.549	0.572	0.892	1066	139.249	110.081	5.10	5.09	5.48	5.51	43.65	47.86
SNT5	1989/10/19 09:50:00.60	953.8	1.290	0.557	1.039	1201	119.503	110.455	5.04	5.09	5.41	5.52	35.21	49.36

Rms, root mean square; TP, third peak.

reported by Stevens *et al.* (2007). Issues with yield uncertainty are common to any method that requires scaling the regional magnitude to $m_b(P)$, excluding uncertainties inherent to $m_b(P)$ itself, such as bias from upper-mantle focusing and (or) defocusing. However, there seems to be another possibility. To convert the global $m_b(P)$ to $m_b(Lg)$ based on Nuttli's regional-wave magnitude equation (Nuttli, 1973), we used a large number of NEqs to calibrate the relations in northeast and northwest China, although these relations may underestimate the size of an explosion in these regions because the *P*-wave energy generated by an explosion can be significantly larger than that excited by a NEq.

EVENT DISCRIMINATION

Using seismic data to discriminate among earthquakes, explosions, and other types of sources remains a difficult but very important task for the nuclear-monitoring community. Theoretically, an isotropic explosion generates mainly *P* waves, whereas an earthquake produced by a shear dislocation mechanism tends to generate relatively strong *S* waves and weaker *P* waves. Therefore, the *P*- and *S*-wave energies that radiate from a seismic source form the basis for determining the properties of the source. Traditionally, this determination relies on the difference between the surface- and body-wave magnitudes. That is, for a seismic event with a given surface-wave magnitude, an explosive source tends to have a larger body-wave magnitude. This constitutes an effective discriminant for distinguishing large events using globally recorded teleseismic data (Stevens and Day, 1985; Fisk *et al.*, 2002; Bonner *et al.*, 2011; Selby *et al.*, 2012). With the values of $m_b(Lg)$ and M_s calculated in the previous section for different types of sources, next, we examined the applicability of the m_b–M_s discriminant to northwest China. As examples, Figure 9 illustrates the m_b–M_s screening criteria suggested by Murphy *et al.* (1997) and Selby *et al.* (2012), in which Figure 9a presents the M_s versus $m_b(Lg)$ relation calculated from regional observations and Figure 9b displays the M_s versus $m_b(P)$ relation, in which the $m_b(P)$ values of the SNTs are from Marshall *et al.* (1985) of the United Kingdom Atomic Weapons Establishment and the $m_b(P)$ values of earthquakes are from the Incorporated Research Institutions for Seismology Data Management Center magnitude catalog. The explosion and earthquake populations apparently overlap in Figure 9a. It is difficult to separate the nuclear tests from the earthquakes using the $m_b(Lg)$–M_s relation, which is consistent with the findings for North Korea nuclear tests (Murphy *et al.*, 2013; Zhao, Xie, Wang, *et al.*, 2017). However, for the $m_b(P)$–M_s relation in Figure 9b, if the screening criteria suggested by Murphy *et al.* (1997) and Selby *et al.* (2012) can be shifted to M_s 1.25; m_b − 3.32 (purple line in Fig. 9b), the nuclear tests can be differentiated from the earthquakes. Therefore, we conclude that the $m_b(Lg)$–M_s relation based on regional observations is an effective

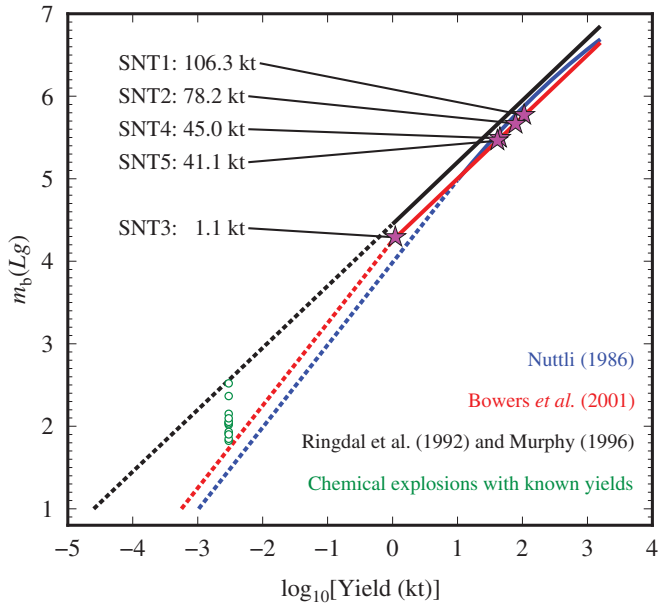

Figure 8. Empirical magnitude–yield relations: The black line is from Ringdal *et al.* (1992) and Murphy (1996), the red line is from Bowers *et al.* (2001), and the blue line is from Nuttli (1986); sections supported by observations are illustrated as solid lines and extrapolations are illustrated as dashed lines. Five previous Semipalatinsk nuclear tests (SNTs; fuchsia stars) and 13 chemical explosions with known yields (green circles) are illustrated.

discriminant for neither the NKTS nor the SNTS, whereas the $m_b(P)$–M_s relation based on global observations is effective if the screening criteria are adjusted appropriately. The unsuccessful application of the $m_b(Lg)$–M_s method with regional data partially results from the difference between the global $m_b(P)$ and the regional $m_b(Lg)$. The events originally used by Nuttli (1973) to calibrate the $m_b(Lg)$ scale were predominantly small earthquakes, whereas the seismic waves of earthquakes are enriched in *S*-wave energy compared to explosions; hence, the magnitudes of nuclear tests, which are inefficient at generating *Lg* waves, may be underestimated.

On the other hand, the *P*/*S* spectral ratio-based method reduces the effects of propagation while highlighting the differences between sources and is thus widely used for identification purposes at regional distances (Taylor *et al.*, 1989; Kim *et al.*, 1993; Walter *et al.*, 1995, 2007; Xie, 2002; Fisk, 2006; Richards and Kim, 2007). We collected *Pn*, *Pg*, *Sn*, and *Lg* waveforms from vertical-component regional seismograms to calculate the *Pg*/*Lg*, *Pn*/*Lg*, and *Pn*/*Sn* spectral ratios for these events in northwest China (Hartse *et al.*, 1997). Various regional phases have different propagation paths, and consequently, it is too complex to correct each phase for attenuation before calculating the *P*/*S* ratio. Therefore, following Zhao *et al.* (2008, 2014), we performed a distance correction only without explicitly correcting for anelastic attenuation. However, the distance correction should include corrections for geometrical spreading and attenuation, albeit in a statistical and implicit way (Zhao *et al.*, 2008, 2014). It appears that this correction can reasonably eliminate the scatter of the results. Then, the distance-corrected ratios were normalized to a reference distance of 500 km, and their network averages were calculated (Walter *et al.*, 1995, 2007; Walter and Taylor, 2001; Zhao *et al.*, 2008; He *et al.*, 2018). Following this procedure, the network-averaged *P*/*S* spectral ratios (*Pg*/*Lg*, *Pn*/*Lg*, and *Pn*/*Sn*) were obtained for the 13 CEx and six NEqs in northwest China, five nuclear tests at the SNTS, and two nearby earthquakes.

The results are analyzed in Figure 10. Figure 10a–c depicts the *Pg*/*Lg*, *Pn*/*Lg*, and *Pn*/*Sn* spectral ratios from a CEx detonated on 6 September 2018, and an earthquake that occurred near the explosion on 20 August 2016. The symbols with faded colors are the observed ratios at individual stations, whereas the color symbols and error bars are the network-averaged values. The network-averaged values are more reliable than the single-station measurements for separating the explosions from nearby earthquakes. Therefore, we averaged the spectral ratios for both the explosions and the earthquakes to create reference curves for event discrimination. The results are shown in Figure 10d–f, in which the light-red symbols are the network-averaged ratios for individual explosions and the light-gray symbols are those for individual earthquakes; the solid symbols and error bars are the averaged values and standard deviations, respectively, for all 13 explosions (brown) and

TABLE 3
Yield Estimation for the Semipalatinsk Nuclear Tests

SNT	1988/04/03	1988/09/14	1988/10/18	1988/12/17	1989/10/19	References
$m_b(P)$	6.10	6.10	4.90	5.90	6.00	AWE
$m_b(Lg)$	6.06	5.97	—	5.80	5.79	Ringdal *et al.* (1992)
	5.77	5.67	4.29	5.50	5.46	This study
Yield (kt)	135	108	—	68	70	Ringdal *et al.* (1992)
	—	140	2.45	84	—	Stevens *et al.* (2007)
	—	94.08	1.17	61.73	—	This study

AWE, Atomic Weapons Establishment; SNT, Semipalatinsk nuclear test.

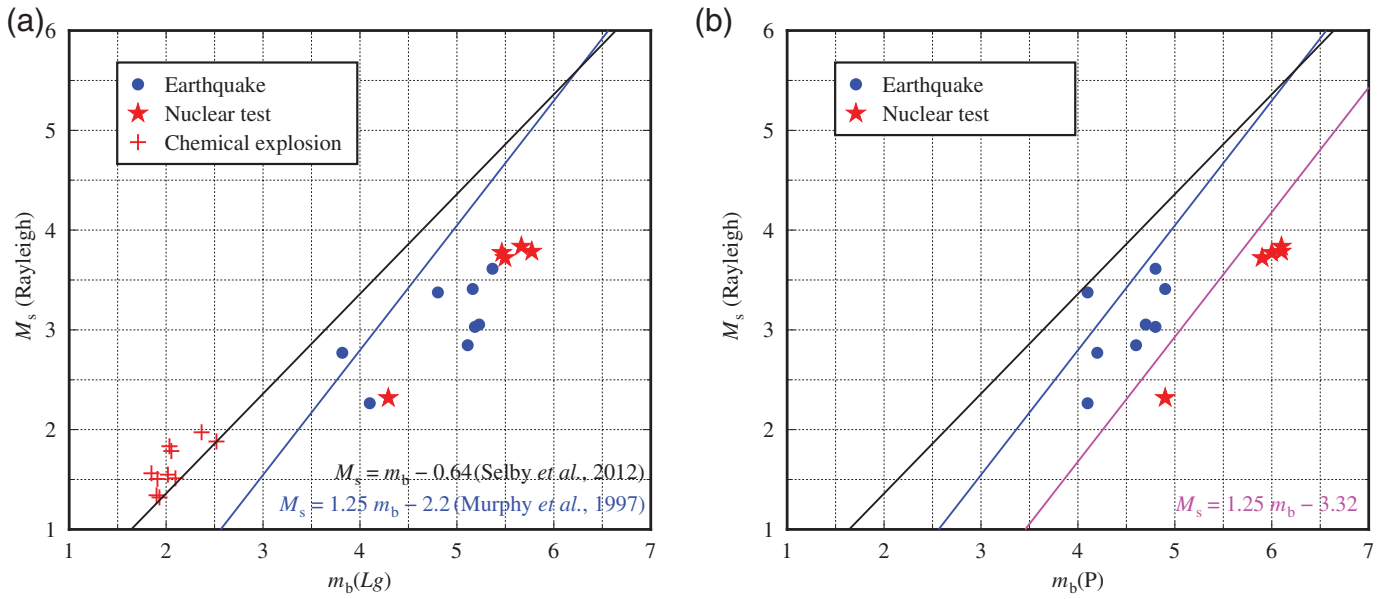

Figure 9. M_s versus m_b for five SNTs (solid red stars), eight natural earthquakes (solid blue circles), and 13 small chemical explosions (red crosses): (a) body-wave magnitudes $m_b(Lg)$ are from regional *Lg* phases and (b) body-wave magnitudes $m_b(P)$ for SNTs are from the United Kingdom Atomic Weapons Establishment (AWE; Marshall *et al.*, 1985), and those for earthquakes are from the Incorporated Research Institutions for Seismology Data Management Center (IRIS DMC) magnitude catalog. The black and blue lines are the screening criteria proposed by Murphy *et al.* (1997) and Selby *et al.* (2012) to distinguish explosions from earthquakes. It appears that the purple line shows a better criterion for the current northwest China dataset.

six nearby earthquakes (blue). For all three types of spectral ratios, the results show that the explosion and earthquake populations can be fully separated by network-measured spectral ratios at frequencies above 2.0 Hz. The reference curves illustrate the difference between the two source types. The spectral ratio method can also be applied to the SNTS to discriminate nuclear tests from nearby earthquakes. Figure 10g–i presents the spectral ratios from the five previous SNTs (red lines) and two nearby earthquakes (green lines). For the historical Semipalatinsk nuclear explosions, the data were recorded by an instrument with a narrow passband, and thus, its frequency response falls by an order of magnitude at 7 Hz. We chose this as the truncation frequency for these historical data. For comparison, the two reference curves from the 13 CEx (brown lines) and six NEqs (blue lines) are also illustrated. The SNTs can be successfully separated from earthquakes near the test site. The previous results suggest that for regional seismic data in northwest China, the *P*/*S* spectral ratio is a reliable discriminant compared with the $m_b(Lg)$–M_s method and is also applicable to large-yield nuclear tests at the SNTS.

In Figure 11, we further compare the *P*/*S* spectral ratios obtained for northwest China with those obtained for northeast China and the Korean Peninsula (He *et al.*, 2018). In the top row (Fig. 11a–c), the solid symbols and error bars are the spectral ratios and standard deviations, respectively, obtained by averaging the network-measured spectral ratios for the five SNTs (red), 13 small CEx (brown), and six NEqs (blue) in northwest China. The bottom row (Fig. 11d–f) shows similar results for six North Korean nuclear tests (red), three small CEx for deep sounding purposes (brown), and four NEqs (blue) in northeast China and the Korean Peninsula (Zhao *et al.*, 2008). The *P*/*S*-type spectral ratios show some common features in both regions. The nuclear explosions show the highest ratios, whereas the NEqs display the lowest ratios. Small CEx with a few tons of charge clearly show higher ratios than NEqs but usually exhibit lower ratios than nuclear explosions. Despite the aforementioned common features, there are also differences between northeast and northwest China. It appears that the ratios in northeast China are generally slightly higher than those in northwest China. If the northeast China results are shifted downward by 0.25 on the logarithmic scale, the results from the two regions can overlap better, although the different types of ratios are not exactly the same; for example, the *Pn*/*Sn* ratios are not as typical as the other two. These features may result from differences in the source regional geology or simply because the data were collected at different epicentral distances. The earlier results demonstrate that even with explosions over a very wide yield range and earthquakes distributed across broad regions, the *P*/*S* spectral ratio method provides a robust discrimination ability between the two source types. At the same time, certain regional variations in *P*/*S* spectral ratio measurements may exist.

DISCUSSION AND CONCLUSIONS

Based on 851 vertical-component seismograms recorded at 122 broadband digital seismic stations in northwest China and its

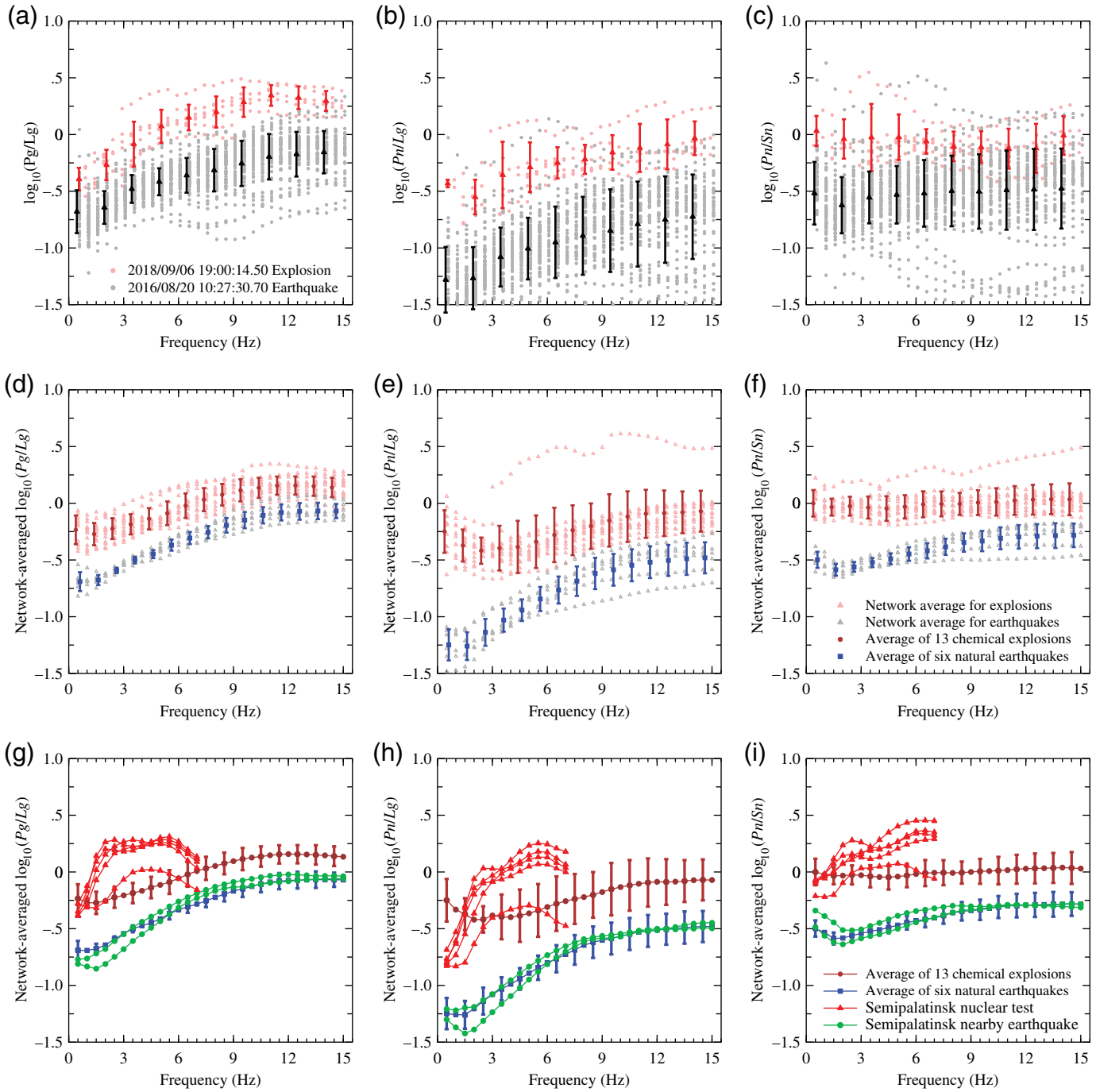

surrounding regions, we investigated the seismic characteristics of different source types, including 13 small CEx in northwest China implemented originally for deep seismic sounding purposes, five underground nuclear tests at the SNTS, and eight NEqs, of which six occurred in northwest China and two were near the SNTS. We used a regional dataset and a broadband *Lg*-wave attenuation model (Zhao *et al.*, 2018) to obtain the *Lg*-wave and Rayleigh-wave magnitudes for all events. However, the obtained $m_b(Lg)$ values were generally lower than the $m_b(P)$ values in both northwest and northeast China. This may be because the original $m_b(Lg)$ scale was

Figure 10. Spectral ratios for selected regional phases. (a–c) Comparisons of the *Pg*/*Lg*, *Pn*/*Lg*, and *Pn*/*Sn* spectral ratios for a chemical explosion (red) and an earthquake (black) near the explosion. Light symbols indicate measurements from individual stations. Solid symbols and error bars show network-averaged values and standard deviations, respectively. (d–f) Spectral ratios for all 13 chemical explosions (brown) and six nearby earthquakes (blue). Light-red symbols are network-averaged ratios for individual explosions and light-gray symbols are network-averaged ratios for individual earthquakes. (g–i) Discrimination results for 13 chemical explosions (brown), six nearby natural earthquakes (blue), five previous nuclear tests (red), and two earthquakes (green) near the SNTS.

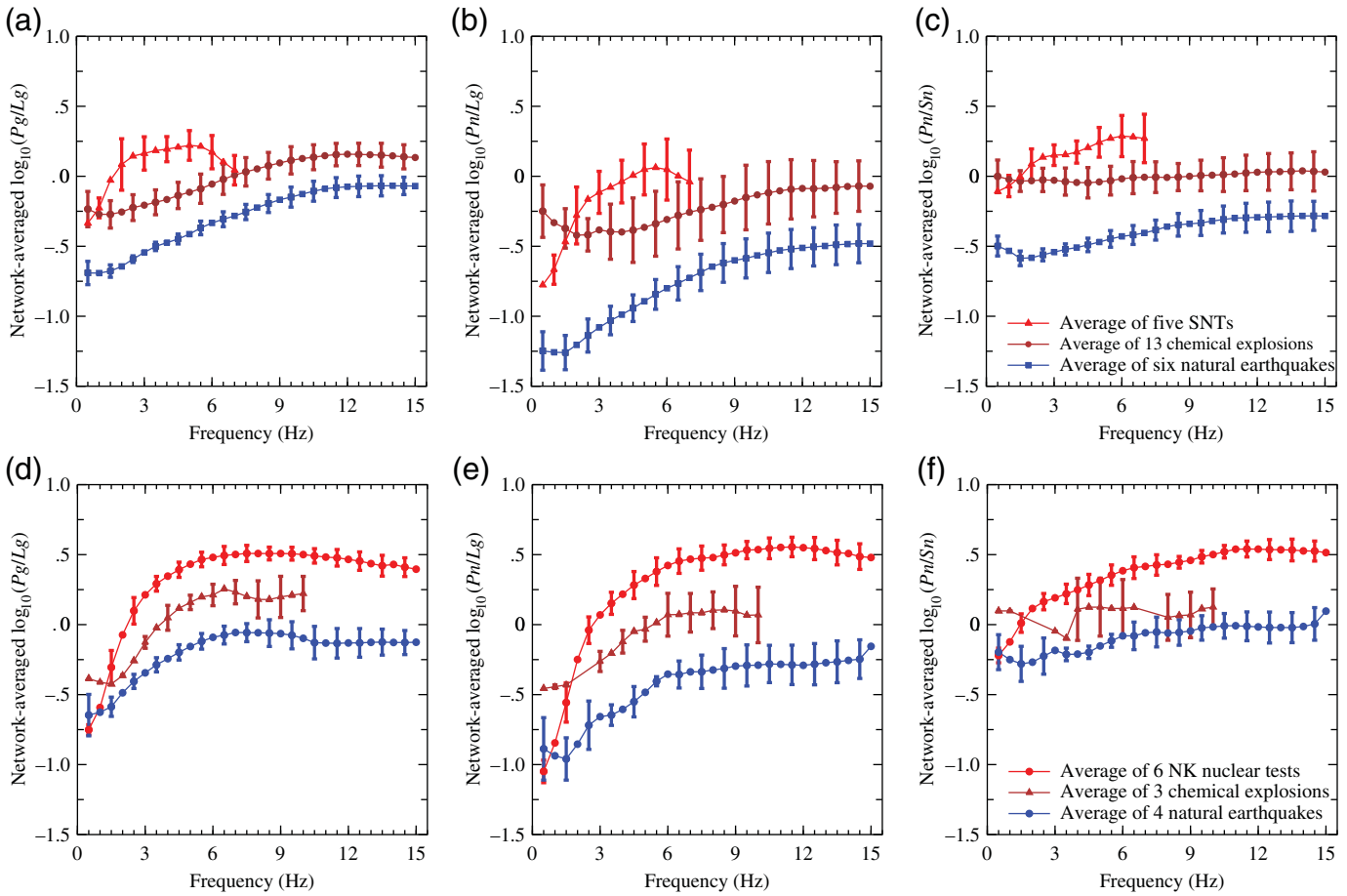

Figure 11. Comparisons of *P*/*S* spectral ratios between different regions. Columns from left to right are *Pg*/*Lg*, *Pn*/*Lg*, and *Pn*/*Sn*. (a–c) Solid symbols and error bars are the average values and standard deviations, respectively, from five SNTs (red), 13 chemical explosions (brown), and six natural earthquakes (blue) in northwest China. (d–f) Similar results for six North Korean (NK) nuclear tests (red), three chemical explosions (brown) (Zhao *et al.*, 2008), and four natural earthquakes in northeast China and the Korean Peninsula (blue) (Zhao *et al.*, 2008).

obtained predominantly from small-magnitude earthquakes, whereas the seismic waves of earthquakes are enriched in *S*-wave energy compared to explosions; hence, the magnitudes of nuclear explosions, which are inefficient at generating *Lg* waves, may be underestimated. Furthermore, other factors may also cause biases between $m_b(P)$ and $m_b(Lg)$, such as a lack of magnitude calibration in northwest China and weak constraints on the magnitude measurements for SNTS events because only historic recordings at WMQ were used here.

We replaced the global $m_b(P)$ with $m_b(Lg)$ to estimate the yields of SNTS tests. Using known-yield small CEx as a constraint at the lower end and considering that central Asia and northwest China are characterized by a stable continental crust, the empirical magnitude–yield relation by Bowers *et al.* (2001) was applied to northwest China and its surrounding regions, including the SNTS. The results are still smaller than the yields from Stevens *et al.* (2007), even with a burial depth correction. The explosions used in this study have the same yield. Therefore, this dataset alone cannot establish a meaningful magnitude–yield relation, especially for much larger nuclear explosions.

Some previous studies have suggested that the m_b–M_s method does not provide an effective discrimination ability in northeast China and the Korean Peninsula when $m_b(Lg)$ is used (Bonner *et al.*, 2008; Chun *et al.*, 2011; Murphy *et al.*, 2013; Zhao, Xie, Wang, *et al.*, 2017). We obtained the same result in northwest China. The unsuccessful application of the m_b–M_s method to regional data again results from the difference between the global $m_b(P)$ and the regional $m_b(Lg)$. On the other hand, the discriminant based on *P*/*S* spectral ratios can successfully differentiate explosions from earthquakes in northwest China as well as the SNTS. Our results indicate that network-based spectral ratios work well at frequencies above 2.0 Hz.

Nuttli (1973) and Ringdal *et al.* (1992) indicated that, due to strong focusing and (or) defocusing effects, the *P* wave is sensitive to lateral heterogeneities in the upper mantle below the test site, resulting in significant uncertainties in the yield estimation. In contrast, *Lg* waves are not affected by lateral heterogeneities in the upper mantle and thus can provide a stable $m_b(Lg)$-based estimation, particularly for small-yield events. However, an explosion source dominantly generates compressional energy. Using the *Lg* wave to characterize an explosion

source implicitly involves an additional factor that converts the compressional energy to shear energy. The conversion mechanism may involve regional geology, local structure, type of source, or even nonlinear near-field processes (e.g., Xie and Lay, 1994; Myers *et al.*, 1999; Patton and Taylor, 2011; Baker *et al.*, 2012), and it is likely linked to the specific test site. To improve the *Lg*-wave-based yield estimates, additional works should be conducted. The SNTS is one of the best calibrated areas in the world using nuclear explosions and multiple chemical calibration shots, and the seismic network has been operational since the 1960s (e.g., Ringdal *et al.*, 1992; Fisk, 2006). Given the wealth of the available data, it is possible to directly calibrate the relation between the yield and $m_b(Lg)$. Another way is to work out a correction factor between the $m_b(Lg)$ and $m_b(P)$. Given the aforementioned complexity, it is likely that the conversion factor is not a simple coefficient. Instead, additional parameters such as the source types and depths as well as local geology could enter into the conversion factor. Therefore, statistics between the two magnitude systems should be combined with the understanding of physical mechanisms underlying the energy conversion.

DATA AND RESOURCES

The waveforms were collected from the China Earthquake Network Center (CENC) and the Data Management Center of China National Seismic Network at the Institute of Geophysics, China Earthquake Administration (SEISDMC, doi: 10.7914/SN/CB) (Zheng *et al.*, 2010) at http://www.seisdmc.ac.cn/ (last accessed December 2019) for those recorded at the China National Digital Seismic Network (CNDSN) and downloaded from the Incorporated Research Institutions for Seismology Data Management Center (IRIS DMC) at www.iris.edu (last accessed February 2020) for the recordings at the Global Seismic Network (GSN) and the International Federation of Digital Seismic Networks (FDSN) stations. Some figures were made using Generic Mapping Tools (GMT; https://forum.generic-mapping-tools.org/, last accessed March 2020) (Wessel *et al.*, 2013).

ACKNOWLEDGMENTS

The authors thank T. Lay for engaging in discussions on this work. The constructive comments from Editor-in-Chief T. Pratt, Associate Editor C. P. Zeiler, and two anonymous reviewers greatly improved this article and are appreciated. This research was supported by the National Key Research and Development Program of China (2017YFC0601206) and the National Natural Science Foundation of China (41630210, 41674060, and 41974061).

REFERENCES

Argo, P., R. A. Clark, A. Douglas, V. Gupta, J. Hassard, P. M. Lewis, P. K. H. Maguire, K. Playford, and F. Ringdal (1995). The detection and recognition of underground nuclear explosions, *Surv. Geophys.* **16,** no. 4, 495–532, doi: 10.1007/Bf00665683.

Baker, G. E., J. L. Stevens, and H. Xu (2012). Explosion shear-wave generation in high-velocity source media, *Bull. Seismol. Soc. Am.* **102,** no. 4, 1301–1319, doi: 10.1785/0120110119.

Barazangi, M., E. Fielding, B. Isacks, and D. Seber (1996). Geophysical and geological databases and CTBT monitoring: A case study of the Middle East, in *Monitoring a Comprehensive Test Ban Treaty*, E. S. Husebye and A. M. Dainty (Editors), Kluwer Academic Publishers, Dordrecht, The Netherlands, 197–224.

Bonner, J., R. B. Herrmann, D. Harkrider, and M. Pasyanos (2008). The surface wave magnitude for the 9 October 2006 North Korean nuclear explosion, *Bull. Seismol. Soc. Am.* **98,** no. 5, 2498–2506, doi: 10.1785/0120080929.

Bonner, J. L., D. R. Russell, D. G. Harkrider, D. T. Reiter, and R. B. Herrmann (2006). Development of a time-domain, variable-period surface-wave magnitude measurement procedure for application at regional and teleseismic distances, part II: Application and M_s–m_b performance, *Bull. Seismol. Soc. Am.* **96,** no. 2, 678–696, doi: 10.1785/0120050056.

Bonner, J. L., A. Stroujkova, and D. Anderson (2011). Determination of Love- and Rayleigh-wave magnitudes for earthquakes and explosions, *Bull. Seismol. Soc. Am.* **101,** no. 6, 3096–3104, doi: 10.1785/0120110131.

Bowers, D., P. D. Marshall, and A. Douglas (2001). The level of deterrence provided by data from the SPITS seismometer array to possible violations of the Comprehensive Test Ban in the Novaya Zemlya region, *Geophys. J. Int.* **146,** no. 2, 425–438, doi: 10.1046/j.1365-246x.2001.01462.x.

Chun, K. Y., Y. Wu, and G. A. Henderson (2011). Magnitude estimation and source discrimination: A close look at the 2006 and 2009 North Korean underground nuclear explosions, *Bull. Seismol. Soc. Am.* **101,** no. 3, 1315–1329, doi: 10.1785/0120100202.

Denny, M., P. Goldstein, K. Mayeda, and W. Walter (1996). Seismic results from DOE's non-proliferation experiment: A comparison of chemical and nuclear explosions, in *Monitoring a Comprehensive Test Ban Treaty*, E. S. Husebye and A. M. Dainty (Editors), Kluwer Academic Publishers, Dordrecht, The Netherlands, 355–364.

Fan, N., L. F. Zhao, X. B. Xie, and Z. X. Yao (2013). Measurement of Rayleigh–wave magnitudes for North Korean nuclear tests, *Chin. J. Geophys.* **56,** no. 3, 906–915, doi: 10.6038/cjg20130319.

Fisk, M. D. (2006). Source spectral modeling of regional *P*/*S* discriminants at nuclear test sites in China and the Former Soviet Union, *Bull. Seismol. Soc. Am.* **96,** no. 6, 2348–2367, doi: 10.1785/0120060023.

Fisk, M. D., D. Jepsen, and J. R. Murphy (2002). Experimental seismic event-screening criteria at the prototype International Data Center, *Pure Appl. Geophys.* **159,** no. 4, 865–888, doi: 10.1007/s00024-002-8662-6.

Gaebler, P., L. Ceranna, N. Nooshiri, A. Barth, S. Cesca, M. Frei, I. Grunberg, G. Hartmann, K. Koch, and C. Pilger (2019). A multi-technology analysis of the 2017 North Korean nuclear test, *Solid Earth* **10,** no. 1, 59–78, doi: 10.5194/se-10-59-2019.

Hartse, H. E., S. R. Taylor, W. S. Phillips, and G. E. Randall (1997). A preliminary study of regional seismic discrimination in central Asia with emphasis on western China, *Bull. Seismol. Soc. Am.* **87,** no. 3, 551–568.

He, X., L. F. Zhao, Z. X. Yao, and X. B. Xie (2018). High-precision relocation and event discrimination for the 3 September 2017 underground nuclear explosion and subsequent seismic events at the North Korean test site, *Seismol. Res. Lett.* **89,** no. 6, 2042–2048, doi: 10.1785/0220180164.

Hong, T. K., C. E. Baag, H. Choi, and D. H. Sheen (2008). Regional seismic observations of the 9 October 2006 underground nuclear explosion in North Korea and the influence of crustal structure on regional phases, *J. Geophys. Res.* **113,** no. B3, 15, doi: 10.1029/2007jb004950.

Kim, W.-Y., and P. G. Richards (2007). North Korean nuclear test: Seismic discrimination at low yield, *Eos Trans. AGU* **88,** no. 14, 158, doi: 10.1029/2007eo140002.

Kim, W.-Y., D. W. Simpson, and P. G. Richards (1993). Discrimination of earthquakes and explosions in the eastern United States using regional high-frequency data, *Geophys. Res. Lett.* **20,** no. 14, 1507–1510, doi: 10.1029/93gl01267.

Koper, K. D. (2020). The importance of regional seismic networks in monitoring nuclear test-ban treaties, *Seismol. Res. Lett.* **91,** no. 2A, 573–580, doi: 10.1785/0220190160.

Marshall, P. D., T. C. Bache, and R. C. Lilwall (1985). Body wave magnitude and location of Soviet underground explosions at the Semipalatinsk test site, *Rept. AWRE No. O 16/84*, HMSO, London.

Marshall, P. D., and P. W. Basham (1973). Rayleigh-wave magnitude scale M, *Pure Appl. Geophys.* **103,** no. 2, 406–414, doi: 10.1007/Bf00876419.

Murphy, J. R. (1996). Types of seismic events and their source descriptions, in *Monitoring a Comprehensive Test Ban Treaty*, E. S. Husebye and A. M. Dainty (Editors), Kluwer Academic Publishers, Dordrecht, The Netherlands, 225–245.

Murphy, J. R., B. W. Barker, and M. E. Marshall (1997). Event screening at the IDC using the M_s/m_b discriminant, *Maxwell Technologies Final Rept.*, 23 pp.

Murphy, J. R., J. L. Stevens, B. C. Kohl, and T. J. Bennett (2013). Advanced seismic analyses of the source characteristics of the 2006 and 2009 North Korean nuclear tests, *Bull. Seismol. Soc. Am.* **103,** no. 3, 1640–1661, doi: 10.1785/0120120194.

Myers, S. C., W. Walter, K. Mayeda, and L. Glenn (1999). Observations in support of Rg scattering as a source for explosion S waves: Regional and local recordings of the 1997 Kazakhstan depth of Burial experiment, *Bull. Seismol. Soc. Am.* 89**,** 544–549.

Nuttli, O. W. (1973). Seismic wave attenuation and magnitude relations for eastern North America, *J. Geophys. Res.* **78,** no. 5, 876–885, doi: 10.1029/JB078i005p00876.

Nuttli, O. W. (1986). Yield estimates of Nevada test site explosions obtained from seismic *Lg* waves, *J. Geophys. Res.* **91,** no. B2, 2137–2151, doi: 10.1029/JB091iB02p02137.

Pasyanos, M. E., and S. C. Myers (2018). The coupled location/depth/yield problem for North Korea's declared nuclear tests, *Seismol. Res. Lett.* **89,** no. 6, 2059–2067, doi: 10.1785/0220180109.

Patton, H. J., and J. Schlittenhardt (2005). A transportable $m_b(Lg)$ scale for central Europe and implications for low-magnitude M_s–m_b discrimination, *Geophys. J. Int.* **163,** no. 1, 126–140, doi: 10.1111/j.1365-246X.2005.02663.x.

Patton, H. J., and S. R. Taylor (2011). The apparent explosion moment: Inferences of volumetric moment due to source medium damage by underground nuclear explosions, *J. Geophys. Res.* **116,** no. B3, doi: 10.1029/2010jb007937.

Richards, P. G., and W. Y. Kim (2007). Seismic signature, *Nature Phys.* **3,** no. 1, 4–6, doi: 10.1038/nphys495.

Ringdal, F., P. D. Marshall, and R. W. Alewine (1992). Seismic yield determination of Soviet underground nuclear explosions at the Shagan River test site, *Geophys. J. Int.* **109,** no. 1, 65–77, doi: 10.1111/j.1365-246X.1992.tb00079.x.

Rougier, E., H. J. Patton, E. E. Knight, and C. R. Bradley (2011). Constraints on burial depth and yield of the 25 May 2009 North Korean test from hydrodynamic simulations in a granite medium, *Geophys. Res. Lett.* **38,** 5, doi: 10.1029/2011gl048269.

Russell, D. R. (2006). Development of a time-domain, variable-period surface-wave magnitude measurement procedure for application at regional and teleseismic distances, part I: Theory, *Bull. Seismol. Soc. Am.* **96,** no. 2, 665–677, doi: 10.1785/0120050055.

Selby, N. D., P. D. Marshall, and D. Bowers (2012). $m_b : M_s$ event screening revisited, *Bull. Seismol. Soc. Am.* **102,** no. 1, 88–97, doi: 10.1785/0120100349.

Shin, J. S., D.-H. Sheen, and G. Kim (2010). Regional observations of the second North Korean nuclear test on 2009 May 25, *Geophys. J. Int.* **180,** no. 1, 243–250, doi: 10.1111/j.1365-246X.2009.04422.x.

Steinberg, D. M., and N. Rabinowitz (2003). Optimal seismic monitoring for event location with application to on site inspection of the Comprehensive Nuclear Test Ban Treaty, *Metrika* **58,** no. 1, 31–57, doi: 10.1007/s001840200222.

Stevens, J. L., G. E. Baker, and H. Xu (2007). The physical basis of the explosion source and generation of regional seismic phases, *Final Rept. for U.S. Air Force contract no. AFRL-VS-HA-TR-2007-0000.*

Stevens, J. L., and S. M. Day (1985). The physical basis of $m_b : M_s$ and variable frequency magnitude methods for earthquake/explosion discrimination, *J. Geophys. Res.* **90,** no. B4, 3009, doi: 10.1029/JB090iB04p03009.

Taylor, S. R., M. D. Denny, E. S. Vergino, and R. E. Glaser (1989). Regional discrimination between NTS explosions and western U.S. earthquakes, *Bull. Seismol. Soc. Am.* **79,** no. 4, 1142–1176.

Voytan, D. P., T. Lay, E. J. Chaves, and J. T. Ohman (2019). Yield estimates for the six North Korean nuclear tests from teleseismic *P* wave modeling and intercorrelation of *P* and *Pn* recordings, *J. Geophys. Res.* **124,** no. 5, 4916–4939, doi: 10.1029/2019jb017418.

Walter, W. R., D. A. Dodge, G. Ichinose, S. C. Myers, M. E. Pasyanos, and S. R. Ford (2018). Body-wave methods of distinguishing between explosions, collapses, and earthquakes: Application to recent events in North Korea, *Seismol. Res. Lett.* **89,** no. 6, 2131–2138, doi: 10.1785/0220180128.

Walter, W. R., E. Matzel, M. E. Pasyanos, D. B. Harris, R. Gok, and S. R. Ford (2007). Empirical observations of earthquake-explosion discrimination using P/S ratios and implications for the sources of explosion *S*-waves, *29th Monitoring Research Review: Ground-Based Nuclear Explosion Monitoring Technologies*, Denver, Colorado, 25–27 September, 684–693.

Walter, W. R., K. M. Mayeda, and H. J. Patton (1995). Phase and spectral ratio discrimination between NTS earthquakes and explosions: 1. Empircal observations, *Bull. Seismol. Soc. Am.* **85,** no. 4, 1050–1067.

Walter, W. R., and S. R. Taylor (2001). A revised magnitude and distance amplitude correction (MDAC2) procedure for regional seismic discriminants: Theory and testing at NTS, *Tech. Rept. UCRL-ID-146882*, doi: 10.2172/15013384.

Wessel, P., W. H. F. Smith, R. Scharroo, J. Luis, and F. Wobbe (2013). Generic Mapping Tools: Improved version released, *Eos Trans. AGU* **94,** 409–410, doi: 10.1002/2013eo450001.

Xie, J. K. (2002). Source scaling of *Pn* and *Lg* spectra and their ratios from explosions in central Asia: Implications for the identification of small seismic events at regional distances, *J. Geophys. Res.* **107,** no. B7, 13, doi: 10.1029/2001jb000509.

Xie, X. B., and T. Lay (1994). The excitation of Lg waves by explosions: A finite-difference investigation, *Bull. Seismol. Soc. Am.* **84,** no. 2, 324–342.

Xie, X. B., and L. F. Zhao (2018). The seismic characterization of North Korea underground nuclear tests, *Chin. J. Geophys.* **61,** no. 3, 889–904, doi: 10.6038/cjg2018L0677.

Yang, X. (2002). A numerical investigation of *Lg* geometrical spreading, *Bull. Seismol. Soc. Am.* **92,** 3067–3079, doi: 10.1785/0120020046.

Zhang, M., and L. X. Wen (2013). High-precision location and yield of North Korea's 2013 nuclear test, *Geophys. Res. Lett.* **40,** no. 12, 2941–2946, doi: 10.1002/grl.50607.

Zhao, L. F., X. B. Xie, X. He, X. Zhao, and Z. X. Yao (2017). Seismological discrimination and yield estimation of the 3 September 2017 Democratic People's Republic of Korea (DPRK) underground nuclear test, *Chin. Sci. Bull.* **62,** no. 35, 4163–4168.

Zhao, L. F., X. B. Xie, W. M. Wang, N. Fan, X. Zhao, and Z. X. Yao (2017). The 9 September 2016 North Korean underground nuclear test, *Bull. Seismol. Soc. Am.* **107,** no. 6, 3044–3051, doi: 10.1785/0120160355.

Zhao, L. F., X. B. Xie, W. M. Wang, J. L. Hao, and Z. X. Yao (2016). Seismological investigation of the 2016 January 6 North Korean underground nuclear test, *Geophys. J. Int.* **206,** no. 3, 1487–1491, doi: 10.1093/gji/ggw239.

Zhao, L. F., X. B. Xie, W. M. Wang, and Z. X. Yao (2008). Regional seismic characteristics of the 9 October 2006 North Korean nuclear test, *Bull. Seismol. Soc. Am.* **98,** no. 6, 2571–2589, doi: 10.1785/0120080128.

Zhao, L. F., X. B. Xie, W. M. Wang, and Z. X. Yao (2012). Yield estimation of the 25 May 2009 North Korean nuclear explosion, *Bull. Seismol. Soc. Am.* **102,** no. 2, 467–478, doi: 10.1785/0120110163.

Zhao, L. F., X. B. Xie, W. M. Wang, and Z. X. Yao (2014). The 12 February 2013 North Korean underground nuclear test, *Seismol. Res. Lett.* **85,** no. 1, 130–134, doi: 10.1785/0220130103.

Zhao, L. F., X. B. Xie, and Z. X. Yao (2018). Crustal *Lg*-wave attenuation in Northwest China and its surrounding areas, *Seismol. Res. Lett.* **89,** no. 2b, 877.

Zheng, X., W. Jiao, C. Zhang, and L. Wang (2010). Short-period Rayleigh-wave group velocity tomography through ambient noise cross-correlation in Xinjiang, northwest China, *Bull. Seismol. Soc. Am.* **100,** no. 3, 1350–1355, doi: 10.1785/0120090225.

Manuscript received 16 April 2020
Published online 20 October 2020